Arginine methylation helps SepIVA balance regulation of septation and elongation in *Mycobacterium smegmatis*

By Angela H Freeman[1], Karen Tembiwa[1], James R Brenner[2], Michael R Chase[3], Sarah M Fortune[3], Yasu S Morita[2], Cara C Boutte[1*]

[1]Department of Biology, University of Texas at Arlington, Arlington, Texas, USA

[2]Department of Microbiology, University of Massachusetts, Amherst, Massachusetts, USA

[3]Department of Immunology and Infectious Disease, Harvard TH Chan School of Public Health, Boston, Massachusetts, USA

[*]corresponding author, cara.boutte@uta.edu

Abstract

Growth of mycobacterial cells requires successful coordination between elongation and division of the cell wall. However, it is not clear which factors directly mediate this coordination. Here, we studied the function and post-translational modification of an essential division factor, SepIVA, in *Mycobacterium smegmatis*. We find that SepIVA is arginine methylated, and that these modifications alter both division and polar elongation of *Msmeg.* Furthermore, SepIVA impacts the localization of MurG.

Polar localization of MurG correlates with polar elongation in arginine methylation mutants of *sepIVA*. These results establish SepIVA as a regulator of both elongation and division, and characterize a physiological role for protein arginine methylation for the first time in bacteria.

Introduction

The cell cycle of rod-shaped bacteria requires coordination of elongation and division. Elongation involves incorporation of newly synthesized cell wall components, such as peptidoglycan (PG) into the existing cell wall. In the well-studied species *B. subtilis* and *E. coli*, this incorporation occurs along the lateral cell wall and is directed by the cytoskeletal factor MreB (1). However, some rod-shaped bacteria, including many Actinobacteria and some Alpha-proteobacteria, lack MreB-like proteins and elongate by incorporating new cell wall near the cell poles (2–7). Polar elongation in mycobacteria, which includes the pathogen *Mycobacterium tuberculosis*, requires the DivIVA protein Wag31 (8–10). Wag31 directs subpolar PG synthesis from its localization site at the cell pole (11) through mechanisms that are currently unclear.

Many essential cell division factors are conserved from *E. coli* to mycobacteria (12, 13). However, because of the distinct features of mycobacteria, such as the extra layers of the cell wall (14), and polar growth (2), we expect that some aspects of cell division must be different as well. In mycobacteria, polar elongation and septation are spatially

coincident but temporally separated; while in lateral growers, elongation and septation are spatially distinct. Because division creates the site of polar growth for the next generation of mycobacterial cells, we expect there to be proteins involved in transitioning between division and elongation, though such factors have not been described.

One structure that is likely shared by the elongation and division processes is the intracellular membrane domain (IMD). The IMD is a membranous hub for generation of lipid-linked cell wall precursors and it localizes to sites of cell wall synthesis: the subpolar region and septum (15). Precursors assembled in the IMD are thought to be translocated into the plasma membrane associated with the cell wall (PM-CW) before assembly into the cell wall (16). Depletion of Wag31 resulted in delocalization of IMD markers (16), suggesting that Wag31 helps define and regulate the IMD. How precursor enzymes associate with the IMD, and how that affects their activity is unknown.

SepIVA is essential for division and interacts with conserved divisome proteins (13, 17). *sepIVA* has also been implicated as a determinant of beta-lactam susceptibility, indicating that it may affect peptidoglycan metabolism (18). Like Wag31, SepIVA comprises a DivIVA domain. DivIVA homologs are often involved in recruitment of other proteins to a site of interest (19–21). Depletion of Wag31 and SepIVA have opposite effects: depletion of SepIVA leads to continued elongation and defective division (13), while depletion of Wag31 leads to elongation arrest (8).

Here, we show that SepIVA is arginine methylated. Arginine methylation is known to be involved in various cell functions in eukaryotes, such as membrane association, protein transport, DNA binding and protein-protein interactions (22, 23). Protein arginine methylation has been identified using mass spectrometry in *E. coli* (24) mycobacteria (25) and *Salmonella* (26). Arginine methylation sites have been shown *in vitro* to affect DNA binding of transcription factors in *Salmonella* (26) and mycobacteria (27). However, protein arginine methylation has never been shown to affect a phenotype of any bacteria.

In this work, we show that arginine methylation on SepIVA regulates SepIVA's localization, PG metabolism, and cell elongation and division. The arginine methylations also affect the localization of PG precursor enzyme MurG. This work establishes SepIVA as a regulator of both elongation and division and demonstrates that arginine methylation has roles beyond modulating DNA binding in bacteria and can critically affect phenotypes such as cell growth and division.

Results

Arginine methylation of SepIVA affects growth and cell length of Msmeg

Post-translational modifications are critical for regulating the physiology of *Mtb* and other mycobacteria (8, 25, 28–33). Most studies thus far have focused on

phosphorylation. To identify proteins that could be regulated by other types of post-translational modification, we re-analyzed a mass spectrometry data set of *Mtb* proteins that we had previously published (30) to search for post translational modification. We found evidence of four arginine methylations on SepIVA (Rv2927c), as well as on many other proteins from *Mtb* (Supplemental table 1).

To see if SepIVA in *M. smegmatis* is also arginine methylated, we immunoprecipitated SepIVA-strep from *Msmeg* lysates and used LCMS-IT-TOF mass spectrometry to measure the post-translational modifications. We found evidence of widespread arginine methylation on SepIVA's 24 arginine residues (Supplemental table 2).

To identify arginine residues in SepIVA for which methylation has a physiological role, we used L5 allele swapping to make several mutants of *sepIVA* in *Msmeg*(34). First, we integrated a wild-type *sepIVA* at the L5 site on a kanamycin-marked vector. Then we deleted the endogenous copy of *sepIVA.* Then, we cloned various *sepIVA* arginine mutants into nourseothricin-marked vectors, and transformed these into the Δ*sepIVA* L5::*sepIVA* WT strain, and selected for allele swaps. Because there were so many arginines with potential methylation sites, we made mutants with several clustered arginines mutated at once. We made R->A alanine mutations to test the function of the arginines and R->K lysine mutations to serve as methyl-ablatives that retain the positive charge on the residue. We found that several groups of arginines were essential for *sepIVA* function, as the alanine mutants did not support growth (R->A mutants, Fig. 1A).

One mutant with arginine to lysine mutations showed that the methylations at the C-terminus were important for normal growth (R->K mutant R224, R228, R230, R234, R254, hereafter called the CT-K mutant) (Fig. 1A) and for normal cell length (Fig. 1B). We were also interested in the arginines at the N-terminus, as the R->K mutant (R3, R19, R31, hereafter called the NT-K mutant) exhibited slightly faster growth than the wild-type, though it was not statistically significant. To further probe the function of the arginine methylations at the C and N termini, we made arginine to methionine mutations at these sites (R->M), as methionine serves as a methyl-mimetic (27). We found the N-terminal methyl-mimetic (hereafter NT-M) had slower growth than the wild-type and shorter cell length (Fig. 1AB), implying that methylation at the N-terminus inhibits growth and cell elongation. The C-terminal methionine mutant was not viable, likely because the protein was unstable (Fig. 1C).

We made all the mutants described above with C-terminal strep tags so we could test for protein stability using western blotting. We found that the non-viable mutants (Fig. 1A) had undetectable levels of SepIVA protein (Fig. 1C). Several of the mutants had significantly higher levels of SepIVA than the wild-type, including the NT-K, NT-M and CT-K mutants (Fig. 1C) which exhibited phenotypes. In order to test whether high levels of these mutant proteins might be responsible for the slow growth, we tested how overexpression of the CT-K mutant – which had the most pronounced growth defect – affected growth rates (Fig. S1). We found that overexpression of SepIVA CT-K did not slow growth in any genetic background. This result shows that the increased protein

levels are not responsible for the slow growth and short cell length of the *sepIVA* CT-K mutant.

These data suggest that the ability to methylate the C-terminus of SepIVA is required for normal growth rate and cell length; however, methylation at the N-terminus appears to slow growth and leads to slightly shorter cells (Fig. 1). For the remainder of this work, we focus on the N and C terminal mutants.

Methylation of SepIVA affects it polar localization

We sought to determine if the arginine methylations could affect SepIVA's localization pattern, which is bright especially at the growing pole (13), and is reminiscent of the localization of some proteins that associate with the Intracellular Membrane Domain (IMD) (11, 15) . To test this, we made merodiploid strains of *Msmeg* with GFPmut3-SepIVA methyl-mutant alleles expressed from the L5 site. We grew these strains in log. phase, and stained the cells with the fluorescent D-amino acid HADA, which preferentially labels sites of new peptidoglycan synthesis (35, 36). Upon imaging the cells, we found that methylation of SepIVA affects its distribution and total intensity (Fig. 2). Specifically, methylation at the N-terminus, in the NT-M mutant, inhibits SepIVA's localization to the fast-growing pole (Fig. 2ACD), as determined by brighter HADA staining. Wild-type cells and mutants that cannot be methylated at the N-terminus (NT-K) have brighter GFPmut3-SepIVA intensity at the fast-growing pole than

the slow-growing pole (Fig. 2CD). The inability to be methylated at the C-terminus, in the CT-K mutant, nearly equalizes SepIVA distribution between the poles (Fig. 2C). Methylation mutants also exhibit differences in GFPmut3-SepIVA intensity broadly (Fig. 2B), but these do not necessarily correlate with western blot results (Fig. 1C), so we cannot conclude whether GFPmut3-SepIVA signal is an indicator of protein stability. Our findings suggest that SepIVA's localization to the cell poles is regulated by methylation on the N-terminus of SepIVA.

Arginine methylation of SepIVA affects PG metabolism

SepIVA's essentiality for cell division and sequence similarity to DivIVA proteins indicates that it regulates the cell wall. To determine if the arginine methylations on SepIVA impact metabolism of cell wall components, we stained the *sepIVA* arginine-mutant strains with HADA (37), which incorporates into the peptidoglycan, and fluorescent trehalose DMN-tre (38), which stains the mycolic acid layer of the cell wall (Fig. 3A). We found that some of the mutants exhibit striking different in HADA staining compared to the wild-type, while we saw only modest different in DMN-tre staining between the strains (Fig. 3BCD). From this we conclude that these mutations of SepIVA affect PG metabolism more directly than MA metabolism. Specifically, methylation at the N-terminus seems to inhibit PG metabolism, as the NT-M mutants exhibit the dimmest HADA staining (Fig. 3BC). Interestingly, the NT-K *sepIVA* mutant, which had brighter

GFPmut3-SepIVA signal at the fast-growing pole also had brighter HADA signal at the poles. SepIVA had previously been shown to be essential for division (13), but these differences in polar staining indicate that SepIVA is also a regulator of polar PG metabolism.

We also observed differences in septal HADA staining between the wild-type and CT-K strain (Fig. 3E). In *sepIVA* wild-type cells, HADA-stained septa are restricted mostly to cells in the larger half of the cell length distribution. However, the CT-K mutants show septal HADA staining in cells of much shorter lengths. The very short average cell lengths in CT-K cell (Fig. 1B) also support the model that, when the C-terminus of SepIVA cannot be methylated, septation is cued at shorter cell lengths. Thus, these arginine methyl-ablative and methyl-mimetic mutants in *sepIVA* impact PG metabolism at both the poles and septa.

Arginine methylation of SepIVA affects polar elongation

To determine if the changes in HADA staining in the *sepIVA* methyl-mutants were due to alterations in the activity of LDT-mediated peptidoglycan remodeling (36) or due to insertion of new peptidoglycan at the cell poles, we measured polar elongation in the *sepIVA* wild-type and mutant strains. We developed a method of measuring elongation using a pulse of HADA (blue), 1.5 hours of outgrowth in media, and another pulse of NADA (green) stain. We then measured the distance of the NADA-stained but

HADA-clear poles, which represents the polar growth during the 1.5-hour outgrowth (Fig. 4A).

First, we used this method to determine if depletion of SepIVA affects cell elongation. SepIVA depletion leads to a slight increase in net polar elongation, with the increase restricted to the slower-growing poles (Fig. 4B). Because cell division is inhibited in the SepIVA-depletion condition, the slower-growing poles there are older than the slower poles in the SepIVA-induced condition. Mycobacterial cell poles typically do not elongate at new poles for a period after division, then begin elongating at the same rate as old poles (39). From these data we conclude that SepIVA is not essential for elongation, and that it is not required for pole maturation.

To determine if methylation of SepIVA could affect elongation, we performed pulse-chase-pulse staining on *sepIVA* wild-type and mutant strains. We found that the NT-M mutant and the CT-K mutant have decreased elongation of both poles, and the NT-K mutant has increase elongation (Fig. 4C). Methylation at the two termini of SepIVA thus appear to have opposite effects on elongation. These results show that SepIVA is an elongation regulator; since it is not required for elongation (Fig. 4B) we conclude that its function may be to help toggle growth between the poles and septum. We observe that HADA staining results match elongation results in the N-terminal mutants: the brighter polar HADA staining (Fig. 3AB) correlated with greater elongation (Fig. 4C). These results suggest that arginine methylation at the N-terminus of SepIVA inhibits polar growth, while lack of methylation stimulates polar growth.

SepIVA affects MurG localization

The IMD is a membrane domain that can be separated by sucrose density centrifugation from the cytoplasmic fractions and from the PM-CW (plasma membrane-cell wall) fraction, which contains PBPs and other periplasmic cell wall enzymes. Our previous study showed that GFPmut3-SepIVA has a similar localization pattern as the IMD-associated arabinogalactan precursor enzyme GlfT2 (13). To determine if SepIVA is associated with the IMD, we performed sucrose gradient fractionation on an *Msmeg* strain with a C-terminal strep tag on SepIVA. We found that SepIVA was found in the cytoplasmic fractions 1-2, as well as fraction 3. GlfT2 was previously shown to be found restricted to the IMD in fractions 4-6 (40). MurG, the final cytoplasmic enzyme in PG precursor synthesis, which also has a typical IMD-localization pattern (11, 16), is found partially in the IMD and partially in the cytoplasmic fractions (16). Thus, SepIVA and MurG have some overlap in their density-gradient distribution. These results show that SepIVA is not associated directly with the IMD; however, its localization pattern indicates that it may associate indirectly or weakly.

Because other DivIVA homologs are involved in recruiting proteins to their site of activity (19, 20), we hypothesized that perhaps SepIVA could be involved in recruiting proteins to its locations near the IMD and at the septum. To test this, we looked at the

effects of SepIVA depletion on localization of GlfT2-mRFP and MurG-Dendra2. We built an *Msmeg* strain where the only copy of *sepIVA* has a C-terminal DAS degradation tag, which targets a protein to be proteolyzed by ClpP when the SspB adaptor is expressed by adding an Atc inducer (13, 41). We transformed this depletion strain with either of the localization constructs. We then added Atc to induce the degradation of SepIVA-DAS, or did not add Atc in the control, and imaged the cells. We found that depletion of SepIVA had little to no effect on GlfT2-mRFP localization (Fig. 5BC). However, we found that MurG-Dendra2 was more evenly distributed in the SepIVA+ control and was in a more punctate pattern in cells induced for *sspB* and depleted for SepIVA (Fig. 5DE). We conclude that SepIVA does not affect IMD structure globally and is not required for IMD-association of GlfT2. Our results indicate, however, that SepIVA could have a role in dispersing MurG from certain sites, or in modulating its stability.

The delocalization of MurG-Dendra2 in the SepIVA-DAS strain was not observed in a SepIVA-DAS strain that did not carry the *sspB* expression plasmid (Fig. S2). Therefore, the delocalization of MurG-Dendra2 is not due to the DAS tag, but likely to leaky expression of SspB in the uninduced condition. These data indicate that MurG-Dendra2 localization is sensitive to subtle changes in SepIVA levels. When SepIVA levels are moderately decreased, MurG-Dendra2 is delocalized and appears cytoplasmic (Fig. 5D, top), but when SepIVA is significantly depleted, MurG-Dendra2 localizes in puncta which could be associated with the IMD (Fig. 5D, bottom).

Arginine methylation of SepIVA affects polar localization of MurG and GlfT2.

We determined that depletion of SepIVA affects localization of MurG and but not GlfT2 (Fig. 5). To determine whether arginine methylation of SepIVA affects MurG or GlfT2 localization, we imaged each fluorescent protein fusion in *sepIVA* wild-type and methyl-mutant strains. According to our results, polar localization of GlfT2-mRFP and MurG-Dendra2 was decreased in the CT-K strain (Fig. 6ACDF). However, the N-terminus does not affect GlfT2-mRFP localization (Fig. 6ABC). Furthermore, MurG's association with the growing pole is decreased in the NT-M strain and increased in the NT-K strain, compared to wild-type (Fig. 6DEF). This suggests that SepIVA that is unmethylated at the N-terminus stimulates MurG's association with the growing pole (Fig 6F), possibly by recruiting it to that site (Fig. 2) and somehow activating it to promote polar PG synthesis (Fig. 3,4).

To ensure that division defects were not due to effects of arginine methylation of SepIVA on the FtsZ ring, we expressed *ftsZ-mcherry2b* in methylation mutants. Our results show that arginine methylation of SepIVA does not affect FtsZ-mcherry2B localization (Fig. S3A).

Discussion

Mycobacteria must regulate not only peptidoglycan precursor synthesis and assembly, but also the flow of precursors for arabinogalactan and mycolic acid

synthesis. Little is known about how the various synthesis pathways for these different cell wall layers are coordinated. However, since the PG layer is the closest to the inner membrane, we expect that PG precursor synthesis is the first to be regulated. Our data indicate that SepIVA is likely directly regulating PG precursor synthesis, which likely has an indirect effect on the other layers including the mycomembrane (Fig. 3B). Our data indicate that SepIVA regulates MurG (Fig. 5,6), which is the final enzyme to work on PG precursors before they are flipped into the periplasm (1, 42), and is therefore an important site of regulation for the PG synthesis pathway. We have yet to determine whether this regulation is direct or indirect.

The IMD is the site of synthesis of lipid-linked cell wall precursors (15, 16) supporting its involvement in both elongation and division. However, we do not currently understand how the IMD is reorganized during the cell cycle to allow for septation and the creation of the new poles. In *E. coli*, MurG interacts with both elongation and division factors (1, 43). We expect this must be the case in mycobacteria as well, and that MurG must need to re-localize at the new IMD at the septum. Our data show that SepIVA is helping to regulate both elongation (Fig.4) and division (Fig. 3F), and that it regulates MurG localization. SepIVA's effects on the localization of MurG could be critical for its function in modulation of both elongation and division.

According to our data, SepIVA depletion results in accumulation or aggregation of MurG. We speculate that SepIVA is somehow affecting MurG's association with the IMD. In *E. coli*, MurG associates with, and depends on the MreBCD proteins for its

localization to sites of elongation (44). It appears that $MurG_{Ec}$ is distributed cytoplasmically in the absence of *mreBCD* (44), similarly to how MurG is apparently distributed cytoplasmically in the *sepIVA*-DAS giles::*sspB* strain (Fig. 5D). This implies that MurG proteins are regulated and localized by cytoplasmic factors, and that they can potentially sometimes be dissociated from the membrane. We expect that a cytoplasmically localized MurG protein would be less active, because it is separated from a high concentration of its substrate, lipid I. Because we also see greater MurG-Dendra2 signal when SepIVA is depleted, it is possible that SepIVA is regulating MurG by destabilizing it or directing it to proteolysis. These may not be separate phenomena. Relocation to the cytoplasm may be sufficient to destabilize a membrane-associated protein.

Regardless of how exactly SepIVA is affecting MurG's localization, our data indicate that arginine methylation on SepIVA is involved in regulating MurG. MurG localization to the pole correlates with polar growth efficiency (Fig. 4, 6). The *sepIVA* NT-K mutant has higher MurG-Dendra2 polar signal (Fig. 6), as well has greater PG metabolism (Fig. 3) and polar growth (Fig. 4) than the wild-type, while the NT-M and CT-K mutants both have less polar MurG-Dendra2 signal as well as less PG metabolism and polar growth (Fig. 3,4,6). The fact that polar localization of MurG is correlated with higher PG metabolism and polar growth also supports the idea that MurG is at the IMD and active when it is localized to the pole. If SepIVA's role in elongation regulation is to regulate MurG's association and dispersal from the IMD

domain at the poles, then it appears that when SepIVA is methylated at the N-terminus, or unmethylated at the C-terminus, it is more active in dispersing MurG from the poles.

Our current model for SepIVA's arginine methylation is that the two poles are methylated and demethylated at different times during the cell cycle. We expect that during polar growth, the N-terminus is unmethylated and the C-terminus is methylated. The unmethylated N-terminus promotes MurG association with the pole (Fig. 6DF) and polar elongation (Fig. 4), while the methylation of the C-terminus inhibits septation (Fig. 1B, 3E). When the cell is ready to begin septation, we expect that it demethylates the C-terminus of SepIVA, and this cues a slowing of elongation (Fig. 4) and initiation of septation (Fig. 3E), possibly partially through re-localization of MurG (Fig. 6). Methylation of the N-terminus (Fig. 4) may occur either to slow polar growth during division, or possibly to inhibit polar growth at the new pole.

Studies on protein arginine methylation done in eukaryotes supports its importance in cell cycle progression (22, 23). Our data establish protein arginine methylation as a regulator of the bacterial cell cycle as well. We have found that the arginine methylation on SepIVA affects both the elongation and division stages of the cell cycle. This work establishes protein arginine methylation as a physiologically important post-translational modification in bacteria and identifies SepIVA as a mediator between the elongation and division processes.

Methods and Materials

Bacterial strains and culture conditions.

Mycobacterium smegmatis (mc^{2}155) was cultured in 7H9 medium (Becton, Dickinson, Franklin Lakes, NJ) with 5 g/L bovine serum albumin (BSA), 2 g/L glucose, 0.85 g/L NaCl, 0.003 g/L catalase, 0.2% glycerol, and 0.05% Tween 80 or plated on LB agar. For *M. smeg* cultures, antibiotic concentrations were: 20 µg/mL nourseothricin, 20 µg/mL zeocin, 20 µg/mL streptomycin, 25 µg/mL kanamycin, 50 µg/mL hygromycin, and 30 µg/mL apramycin. For *E. coli* cultures, antibiotic concentrations were: 40 µg/mL nourseothricin, 25 µg/mL zeocin, 50 µg/mL streptomycin, 50 µg/mL kanamycin, 100 µg/mL hygromycin, and 50 µg/mL apramycin *E. coli* TOP10 or DH5α were used for cloning.

Strain construction

Because it is essential in *M. smegmatis, sepIVA* mutants were constructed by first integrating an additional copy of *sepIVA* at the L5 integration site. After complementing *sepIVA* at the L5 site, *sepIVA* at its native locus was knocked out via recombineering (45), as previously described (31). Mutant copies of *sepIVA* replaced wildtype *sepIVA* at the L5 site via allelic exchange (34, 46).

sepIVA depletion strains were constructed as previously described (13). Merodiploid expression constructs of GlfT2-mRFP, FtsZ-mcherry2B, and MurG-Dendra2 were integrated at the Tweety integrase site (47). The merodiploid construct

expressing GFPmut3-SepIVA was integrated at the L5 integrase site. All strains used are listed in Table S3 of the supplementary material, along with plasmids listed in Table S4 and primers listed in Table S5.

Growth rate assay

Biological replicates of *sepIVA* arginine mutants were grown to log phase in 7H9 medium. Cultures were diluted to OD_{600} = 0.1 in 200 µL 7H9 medium in a non-treated 96-well plate. Optical density at 600 nm was measured over the next 18-24 hours using a plate reader (BioTek Synergy neo2 multi-mode reader) at 37°C, shaking continuously. Population doubling times were determined using the exponential growth equation and least squares regression fitting method in GraphPad Prism (version 9.2). P values were calculated using ordinary one-way ANOVA, Dunnett's multiple comparisons test, with a single pooled variance.

Western blots

Log phase cultures (10 mL) were pelleted and resuspended in 500 µL PBS + 1 mM phenylmethylsulfonyl fluoride (PMSF). Cells were lysed using glass beads (MiniBeadBeater-16, model 607, Biospec). Supernatants from cell lysates were run on 4–12% NuPAGE Bis Tris precast gels (Life Technologies, Beverley, MA) using MES running buffer (Life Technologies, Beverly, MA). Proteins were transferred onto polyvinylidene difluoride (PVDF) membranes (GE Healthcare). Strep-tagged proteins

were detected using rabbit anti-Strep-tag II antibody (1:1000, Abcam, ab76949) in Tris-buffered saline with Tween 20 (TBST) with 0.5% BSA and goat anti-rabbit IgG (H+L) horseradish peroxide (HRP)-conjugated secondary antibody (1:10,000, Thermo Fisher Scientific 31460) in TBST.

Microscopy

Cells were imaged using a Nikon Ti-2 widefield epifluorescence microscope with a Photometrics Prime 95B camera and a Plan Apo 100X, 1.45 -numerical-aperture (NA) lens objective. Green-fluorescent images for GFPmut3 or Dendra2 localization or DMN-tre staining were taken with a 470/40nm excitation filter and a 525/50nm emission filter. Blue-fluorescent images for HADA staining were taken with a 350/50nm excitation filter and a 460/50nm emission filter. Red-fluorescent images for mRFP and mcherry2B localization were taken with a 560/40nm excitation filter and a 630/70 emission filter. Images were captured using NIS Elements software. Images were analyzed using FIJI and MicrobeJ (48). For cell detection using MicrobeJ, parameters for width and area were set. V-snapping cells were cut at the septum so daughter cells could be detected as individual cells. Overlapping cells were excluded from analysis.

Cell lengths, mean intensities, maximum intensities and minimum intensities of at least 250 cells per genotype were quantified using MicrobeJ. Mean intensity profiles were plotted using the “XStatProfile” plotting tool in MicrobeJ. P-values were calculated

using ordinary one-way ANOVA, Dunnett's multiple comparisons test, with a single pooled variance using GraphPad Prism (v9.2).

Localization of cell wall proteins upon SepIVA depletion.

For depletion of SepIVA, log phase cells (10 mL) were incubated (37°C) with 500 ng/mL Anhydrotetracycline (ATc) for 7-9 hours. For induction of GlfT2-mRFP, 1 ng/mL IVN were added, and cells were incubated (37°C) for 5 hours. Cells were fixed for microscopy. Cells were fixed for microscopy with 1.6% paraformaldehyde for 10 minutes and then washed and resuspended in PBS tween80. Microscopy images were analyzed in ImageJ and MicrobeJ. P-values calculated by unpaired t-test using GraphPad Prism (v9.2).

Fluorescent staining

HADA and NADA fluorescent D-alanine amino acids were used to stain the peptidoglycan cell wall layer (35). For PG analysis, HADA stain was added to 1 mL exponentially growing cells at a final concentration of 1 ug/mL for 2 minutes at room temperature before washing twice in PBST. For pulse-chase experiments, HADA (1 ug/mL) was added for 10 minutes before cells were washed twice in 7H9, incubated (37°C) for 2 hours, and stained again using NADA (1 ug/mL) for 2 minutes. Cells were washed twice in PBST and imaged. Images were analyzed in ImageJ (NIH). The length of the poles and the length of the entire cell were measured manually for each cell.

DMN-tre stain was used to visualize the trehalose mycolic acid layer of the cell wall (38). DMN-tre stain was added to 500 µL log phase culture at final concentration 1 µg/mL. Cultures were incubated (37°C) for 30 minutes, washed once with 7H9 and once with PBST before imaging.

Sucrose Density Gradient Fractionation

Sucrose density gradient fractionation was performed as previously described (15). In brief, cells were grown to log phase and lysed by nitrogen cavitation. Lysate was then placed on top of a 20-50% sucrose gradient and centrifuged at 35,000 rpm for 6 hours at 4°C. Twelve one-mL fractions were collected and analyzed.

Immunoprecipitation and mass spectrometry

We previously performed LCQ-MS/MS to identify peptides from *Mtb* cell lysates (30). Here, we re-analyzed those data to search for modifications in peptides, using Andromeda software.

SepIVA-strep was immunoprecipitated from CB1223. Cells were grown to late log. phase, pelleted and frozen. Cell pellets were resuspended in PBS with PMSF at 1 mM, lysed by bead beating, and clarified by centrifugation. Immunoprecipitation was performed with MagStrep type 3 XT beads (Iba Life Sciences, Gottingen, Germany) according to the manufacturers protocol. Liquid was evaporated from the immunoprecipitants, and then digested by Trypsin/Lys-C Mix, Mass Spec Grade

protease (Promega), according to the manufacturer's protocols for reduction, alkylation and two-step in-solution digestion of proteolytically resistant proteins. The digested peptide solution was then cleaned by C18-Ziptips (Sigma Aldrich) according to the manufacturers protocol.

LC-MS analysis was performed on LTQ Velos pro mass spectrometer (Thermo Scientific, CA, USA) combined with a UHPLC (UltiMate 3000, Dionex, USA). The digested peptides were separated by a nano viper analytical C18 column. (Acclaim pepMap, 150 mm × 75μm, 2μm, 100 Å, Thermo Scientific, CA, USA). A 60 min gradient method was used to separate the digested peptides (0–3 min 4.0%B, 3–50 min 4.0–50.0% B, 50–50.1 min 50–90% B,50.1–55 min 90% B, 55–55.1 min 90–4% B, 55.1–60 min 4% B; mobile phase A: 0.1% FA in water; mobile phase B: 0.1% FA in 95% acetonitrile, 5% water). 5μL of digested samples was injected at 300 nL/min flow. The nano-electrospray ionization (ESI) source used with a fixed spray voltage at 2.4 kV and a heated capillary temperature at 275 °C. A full MS spectrum obtained in normal scan mode from 350 to 2000 m/z mass range. The data-dependent acquisition was performed to get the MS/MS spectra for the 5 most abundant ions. The software Proteome Discoverer (Thermo Scientific, USA) was used to search and identify the peptides. LC-MS was performed at the Shimadzu Center for Advanced Analytical Chemistry at UT Arlington.

Acknowledgements

This work was funded by grant R15GM131317 from the NIH. We thank Heather Lake who contributed to optimization of some experiments, and Arash Emami Saleh who aided in data processing.

References

1. Egan AJF, Errington J, Vollmer W. 2020. Regulation of peptidoglycan synthesis and remodelling. Nat Rev Microbiol https://doi.org/10.1038/s41579-020-0366-3.

2. Thanky NR, Young DB, Robertson BD. 2007. Unusual features of the cell cycle in mycobacteria: Polar-restricted growth and the snapping-model of cell division. Tuberculosis 87:231–236.

3. Aldridge BB, Fernandez-Suarez M, Heller D, Ambravaneswaran V, Irimia D, Toner M, Fortune SM. 2012. Asymmetry and Aging of Mycobacterial Cells Lead to Variable Growth and Antibiotic Susceptibility. Science 335:100–104.

4. Brown PJB, de Pedro MA, Kysela DT, Van der Henst C, Kim J, De Bolle X, Fuqua C, Brun YV. 2012. Polar growth in the Alphaproteobacterial order Rhizobiales. Proceedings of the National Academy of Sciences 109:1697–1701.

5. Cameron TA, Zupan JR, Zambryski PC. 2015. The essential features and modes of bacterial polar growth. Trends in Microbiology 23:347–353.

6. Zupan JR, Grangeon R, Robalino-Espinosa JS, Garnica N, Zambryski P. 2019. GROWTH POLE RING protein forms a 200-nm-diameter ring structure essential for polar growth and rod shape in Agrobacterium tumefaciens. PNAS 201905900.

7. Zupan J, Guo Z, Biddle T, Zambryski P. 2021. *Agrobacterium tumefaciens* Growth Pole Ring Protein: C Terminus and Internal Apolipoprotein Homologous Domains Are Essential for Function and Subcellular Localization. mBio 12:e00764-21, /mbio/12/3/mBio.00764-21.atom.

8. Kang C-M, Nyayapathy S, Lee J-Y, Suh J-W, Husson RN. 2008. Wag31, a homologue of the cell division protein DivIVA, regulates growth, morphology and polar cell wall synthesis in mycobacteria. Microbiology 154:725–735.

9. Kang C-M. 2005. The Mycobacterium tuberculosis serine/threonine kinases PknA and PknB: substrate identification and regulation of cell shape. Genes & Development 19:1692–1704.

10. Melzer ES, Sein CE, Chambers JJ, Sloan Siegrist M. 2018. DivIVA concentrates mycobacterial cell envelope assembly for initiation and stabilization of polar growth. Cytoskeleton 75:498–507.

11. Meniche X, Otten R, Siegrist MS, Baer CE, Murphy KC, Bertozzi CR, Sassetti CM. 2014. Subpolar addition of new cell wall is directed by DivIVA in mycobacteria. Proceedings of the National Academy of Sciences 111:E3243–E3251.

12. Hett EC, Rubin EJ. 2008. Bacterial Growth and Cell Division: a Mycobacterial Perspective. Microbiology and Molecular Biology Reviews 72:126–156.

13. Wu KJ, Zhang J, Baranowski C, Leung V, Rego EH, Morita YS, Rubin EJ, Boutte CC. 2018. Characterization of Conserved and Novel Septal Factors in *Mycobacterium smegmatis*. Journal of Bacteriology 200:e00649-17, /jb/200/6/e00649-17.atom.

14. Jankute M, Cox JAG, Harrison J, Besra GS. 2015. Assembly of the Mycobacterial Cell Wall. Annual Review of Microbiology 69:405–423.

15. Hayashi JM, Luo C-Y, Mayfield JA, Hsu T, Fukuda T, Walfield AL, Giffen SR, Leszyk JD, Baer CE, Bennion OT, Madduri A, Shaffer SA, Aldridge BB, Sassetti CM, Sandler SJ, Kinoshita T, Moody DB, Morita YS. 2016. Spatially distinct and metabolically active membrane domain in mycobacteria. PNAS 113:5400–5405.

16. García-Heredia A, Kado T, Sein CE, Puffal J, Osman SH, Judd J, Gray TA, Morita YS, Siegrist MS. 2021. Membrane-partitioned cell wall synthesis in mycobacteria. eLife 10:e60263.

17. Jain P, Malakar B, Khan MZ, Lochab S, Singh A, Nandicoori VK. 2018. Delineating FtsQ-mediated regulation of cell division in *Mycobacterium tuberculosis*. Journal of Biological Chemistry 293:12331–12349.

18. Flores AR, Parsons LM, Pavelka MS. 2005. Characterization of Novel Mycobacterium tuberculosis and Mycobacterium smegmatis Mutants Hypersusceptible to -Lactam Antibiotics. Journal of Bacteriology 187:1892–1900.

19. Marston AL, Errington J. 1999. Selection of the midcell division site in Bacillus subtilis through MinD-dependent polar localization and activation of MinC. Molecular Microbiology 33:84–96.

20. Halbedel S, Lewis RJ. 2019. Structural basis for interaction of DivIVA/GpsB proteins with their ligands. Molecular Microbiology 111:1404–1415.

21. Hammond LR, Khan SJ, Sacco MD, Spanoudis C, Hough A, Chen Y, Eswara PJ. 2021. GpsB coordinates cell division and cell surface decoration by wall teichoic acids in *Staphylococcus aureus*. preprint, Microbiology.

22. Raposo AE, Piller SC. 2018. Protein arginine methylation: an emerging regulator of the cell cycle. Cell Div 13:3.

23. Biggar KK, Li SS-C. 2015. Non-histone protein methylation as a regulator of cellular signalling and function. Nat Rev Mol Cell Biol 16:5–17.

24. Zhang M, Xu J-Y, Hu H, Ye B-C, Tan M. 2018. Systematic Proteomic Analysis of Protein Methylation in Prokaryotes and Eukaryotes Revealed Distinct Substrate Specificity. PROTEOMICS 18:1700300.

25. Sakatos A, Babunovic GH, Chase MR, Dills A, Leszyk J, Rosebrock T, Bryson B, Fortune SM. 2018. Posttranslational modification of a histone-like protein regulates phenotypic resistance to isoniazid in mycobacteria. Science Advances 4:eaao1478.

26. Su Y, Li J, Zhang W, Ni J, Huang R, Wang Z, Cheng S, Wang Y, Tian Z, Zhou Q, Lin D, Wu W, Tang CM, Liu X, Lu J, Yao Y-F. 2021. Methylation of PhoP by CheR Regulates *Salmonella* Virulence. mBio https://doi.org/10.1128/mBio.02099-21.

27. Singhal A, Virmani R, Naz S, Arora G, Gaur M, Kundu P, Sajid A, Misra R, Dabla A, Kumar S, Nellissery J, Molle V, Gerth U, Swaroop A, Sharma K, Nandicoori VK, Singh Y. 2020. Methylation of two-component response regulator MtrA in mycobacteria negatively modulates its DNA binding and transcriptional activation. Biochemical Journal 477:4473–4489.

28. Prisic S, Husson RN. 2014. Mycobacterium tuberculosis Serine/Threonine Protein Kinases. Microbiology Spectrum 2.

29. Prisic S, Dankwa S, Schwartz D, Chou MF, Locasale JW, Kang C-M, Bemis G, Church GM, Steen H, Husson RN. 2010. Extensive phosphorylation with overlapping specificity by Mycobacterium tuberculosis serine/ threonine protein kinases. Proceedings of the National Academy of Sciences 107:7521–7526.

30. Garces A, Atmakuri K, Chase MR, Woodworth JS, Krastins B, Rothchild AC, Ramsdell TL, Lopez MF, Behar SM, Sarracino DA, Fortune SM. 2010. EspA Acts

as a Critical Mediator of ESX1-Dependent Virulence in Mycobacterium tuberculosis by Affecting Bacterial Cell Wall Integrity. PLOS Pathogens 6:e1000957.

31. Boutte CC, Baer CE, Papavinasasundaram K, Liu W, Chase MR, Meniche X, Fortune SM, Sassetti CM, Ioerger TR, Rubin EJ. 2016. A cytoplasmic peptidoglycan amidase homologue controls mycobacterial cell wall synthesis. eLife 5.

32. Iswahyudi, Mukamolova GV, Straatman-Iwanowska AA, Allcock N, Ajuh P, Turapov O, O'Hare HM. 2019. Mycobacterial phosphatase PstP regulates global serine threonine phosphorylation and cell division. Sci Rep 9:8337.

33. Shamma F, Papavinasasundaram K, Quintanilla SY, Bandekar A, Sassetti C, Boutte CC. 2020. Phosphorylation on PstP Regulates Cell Wall Metabolism and Antibiotic Tolerance in *Mycobacterium smegmatis*. J Bacteriol 203:e00563-20, /jb/203/4/JB.00563-20.atom.

34. Pashley CA, Parish T. 2003. Efficient switching of mycobacteriophage L5-based integrating plasmids in *Mycobacterium tuberculosis*. FEMS Microbiology Letters 229:211–215.

35. Kuru E, Hughes HV, Brown PJ, Hall E, Tekkam S, Cava F, de Pedro MA, Brun YV, VanNieuwenhze MS. 2012. In Situ Probing of Newly Synthesized Peptidoglycan in

Live Bacteria with Fluorescent D -Amino Acids. Angewandte Chemie International Edition 51:12519–12523.

36. Baranowski C, Welsh MA, Sham L-T, Eskandarian HA, Lim HC, Kieser KJ, Wagner JC, McKinney JD, Fantner GE, Ioerger TR, Walker S, Bernhardt TG, Rubin EJ, Rego EH. 2018. Maturing Mycobacterium smegmatis peptidoglycan requires non-canonical crosslinks to maintain shape. eLife 7:e37516.

37. Kuru E, Tekkam S, Hall E, Brun YV, Van Nieuwenhze MS. 2015. Synthesis of fluorescent D-amino acids and their use for probing peptidoglycan synthesis and bacterial growth in situ. Nat Protoc 10:33–52.

38. Kamariza M, Shieh P, Ealand CS, Peters JS, Chu B, Rodriguez-Rivera FP, Sait MRB, Treuren WV, Martinson N, Kalscheuer R, Kana BD, Bertozzi CR. 2018. Rapid detection of Mycobacterium tuberculosis in sputum with a solvatochromic trehalose probe. Science Translational Medicine 10:eaam6310.

39. Hannebelle MTM, Ven JXY, Toniolo C, Eskandarian HA, Vuaridel-Thurre G, McKinney JD, Fantner GE. 2020. A biphasic growth model for cell pole elongation in mycobacteria. Nat Commun 11:452.

40. Hayashi JM, Richardson K, Melzer ES, Sandler SJ, Aldridge BB, Siegrist MS, Morita YS. 2018. Stress-Induced Reorganization of the Mycobacterial Membrane Domain. mBio 9.

41. Kim J-H, Wei J-R, Wallach JB, Robbins RS, Rubin EJ, Schnappinger D. 2011. Protein inactivation in mycobacteria by controlled proteolysis and its application to deplete the beta subunit of RNA polymerase. Nucleic Acids Res 39:2210–2220.

42. Gee CL, Papavinasasundaram KG, Blair SR, Baer CE, Falick AM, King DS, Griffin JE, Venghatakrishnan H, Zukauskas A, Wei J-R, Dhiman RK, Crick DC, Rubin EJ, Sassetti CM, Alber T. 2012. A Phosphorylated Pseudokinase Complex Controls Cell Wall Synthesis in Mycobacteria. Sci Signal 5:ra7–ra7.

43. Laddomada F, Miyachiro MM, Dessen A. 2016. Structural Insights into Protein-Protein Interactions Involved in Bacterial Cell Wall Biogenesis. Antibiotics (Basel) 5:14.

44. Mohammadi T, Karczmarek A, Crouvoisier M, Bouhss A, Mengin-Lecreulx D, den Blaauwen T. 2007. The essential peptidoglycan glycosyltransferase MurG forms a complex with proteins involved in lateral envelope growth as well as with proteins involved in cell division in Escherichia coli. Mol Microbiol 65:1106–1121.

45. van Kessel JC, Hatfull GF. 2008. Mycobacterial Recombineering. Methods in Molecular Biology (Clifton, NJ) 435:203–215.

46. Kieser KJ, Boutte CC, Kester JC, Baer CE, Barczak AK, Meniche X, Chao MC, Rego EH, Sassetti CM, Fortune SM, Rubin EJ. 2015. Phosphorylation of the

Peptidoglycan Synthase PonA1 Governs the Rate of Polar Elongation in Mycobacteria. PLOS Pathogens 11:e1005010.

47. Pham TT, Jacobs-Sera D, Pedulla ML, Hendrix RW, Hatfull GFY 2007. Comparative genomic analysis of mycobacteriophage Tweety: evolutionary insights and construction of compatible site-specific integration vectors for mycobacteria. Microbiology 153:2711–2723.

48. Ducret A, Quardokus EM, Brun YV. 2016. MicrobeJ, a tool for high throughput bacterial cell detection and quantitative analysis. Nature Microbiology 1:16077.

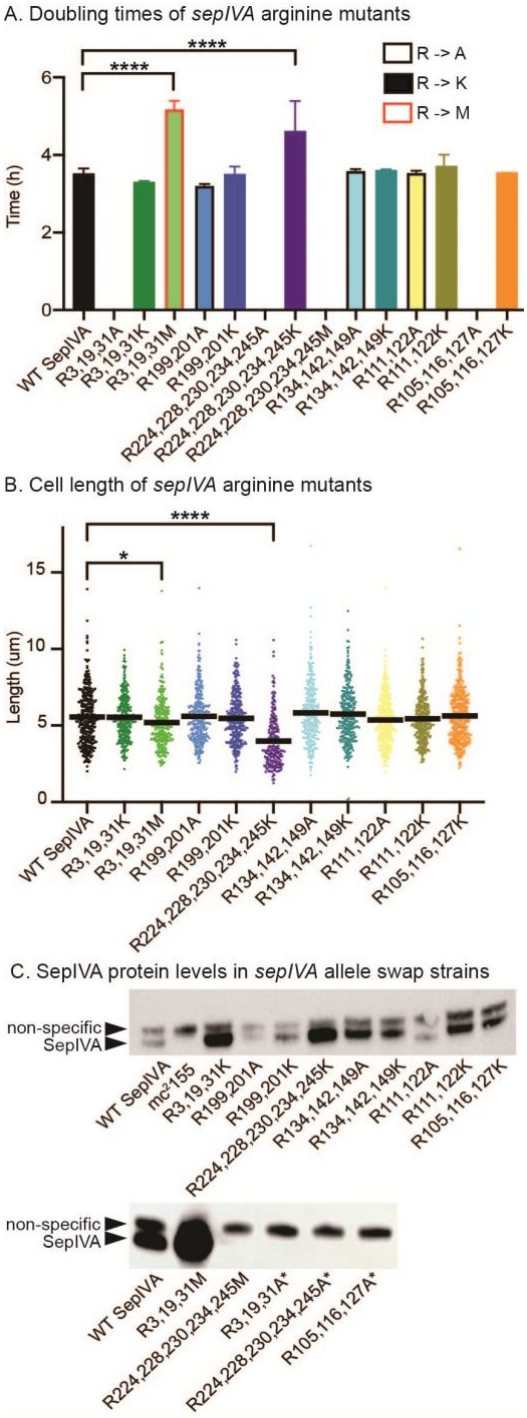

Figure 1. Arginine methylation of SepIVA affects growth and cell length of *M.smeg.*

(A) Doubling time of *M. smeg* cells expressing WT or arginine methylation mutants of SepIVA. Black outline, lighter color bars represent arginine to alanine mutants. No outline, darker color bars represent methyl-ablative mutants. Red outline bars represent methyl-mimetic mutants. Strains without bars were non-viable. At least 3 biological replicates of each strain were used. Error bars represent standard deviation. ****, *P = <0.0001.*

(B) Cell lengths of SepIVA WT and arginine methylation mutants. Bars represent mean. At least 300 cells over three biological replicates of each strain were analyzed. *, *P = 0.0439;* ****, *P = <0.0001.*

(C) α-strep western blot of L5::*sepIVA*-strep WT or arginine methylation mutants. mc^2155 without a strep tag was used as a negative control (lane 2). '*' denotes merodiploid strains. The non-specific band serves as a loading control.

644

645

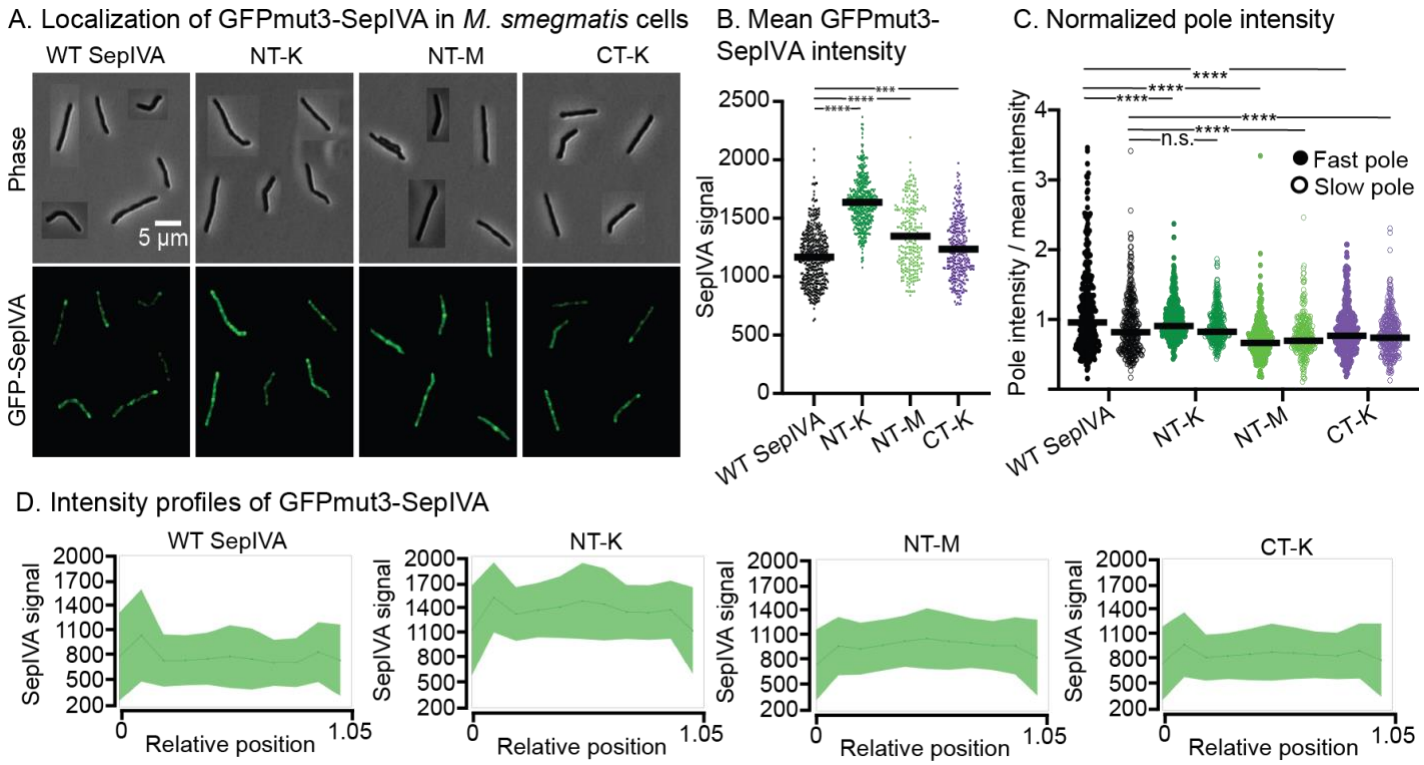

Figure 2. Methylation of SepIVA affects its polar localization. (A) Images of *M. smeg* cells expressing L5::*GFPmut3-sepIVA* WT and arginine methylation mutants. Strains are merodiploid. Phase images are on the top. Fluorescent images are on the bottom. Scale bar applies to all images. Images of several cells were cropped together. **(B)** Mean intensity values of 250+ cells expressing L5::*GFPmut3-sepIVA* WT and arginine methylation mutants. Bar represents mean intensity value between cells. The adjusted p-values of each mutant compared to the WT are: NT-K = <0.0001; NT-M = <0.0001; and CT-K = 0.0002. Three biological replicate strains were imaged for each genotype. **(C)** Normalized intensity of poles of cells expressing L5::*GFPmut3-sepIVA* WT and arginine methylation mutants. Each dot represents ratio of pole intensity value over mean intensity value of the cell. Filled in dots represent the faster (brighter) growing pole, empty dots represent the slower (dimmer) growing pole. Bar represents median intensity value. At least 250+ cells across three biological replicates of each mutant were used. The adjusted p-values of the mutant fast poles compared to the WT fast pole are: NT-K = <0.0001; NT-M = <0.0001; and CT-K = <0.0001. The adjusted p-values of the mutant slow poles compared to the WT slow pole are: NT-K = 0.9510; NT-

M = <0.0001; and CT-K = <0.0001. **(D)** Intensity profiles of GFP-SepIVA signal of WT and methylation mutants. The solid line represents the mean intensity value, and the shaded area represents standard deviation. At least 250+ cells across three biological replicates of each mutant were analyzed in MicrobeJ. P-values were calculated using ordinary one-way ANOVA, Dunnett's multiple comparisons test, with a single pooled variance in GraphPad Prism (v9.2).

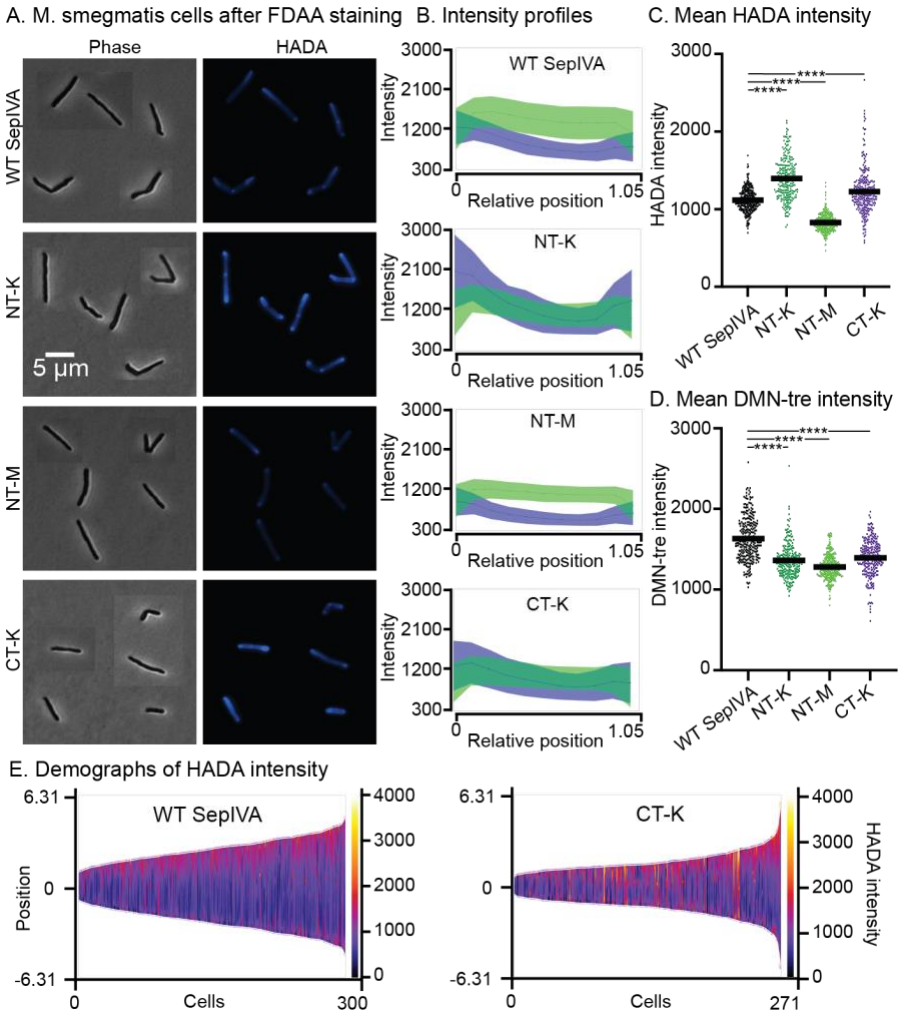

Figure 3. Arginine Methylation of SepIVA affects PG metabolism. (A) Images of M. smeg cells expressing *L5::sepIVA* WT and arginine methylation mutants. Pictures of several cells from images processed identically were pasted together. Scale bar applies

to all images. **(B)** Intensity profiles of HADA (blue) and DMN-tre (green) signal of WT and methylation mutants. The solid line represents the mean intensity value, and the shaded area represents standard deviation. At least 250+ cells across three biological replicates of each mutant were analyzed in MicrobeJ. Cells were pole-sorted such that the brighter pole in the HADA channel was set to 0 on the X axis. **(C and D)** Mean HADA **(C)** and DMN-tre **(D)** intensity values of M. smeg cells expressing *L5::sepIVA* WT and arginine methylation mutants. Bar represents mean intensity value. ****, P = <0.0001. P-values were calculated using ordinary one-way ANOVA, Dunnett's multiple comparisons test, with a single pooled variance in GraphPad Prism (v9.2). **(E)** Demographs of HADA intensity across the length of the cell of WT SepIVA and CT-K mutant. Demographs for other methylation mutants can be found in supplemental figure 2. At least 250+ cells across three biological replicates of each mutant were analyzed in MicrobeJ. Cells were pole-sorted such that the brighter pole in the HADA channel was oriented to the top along the Y axis.

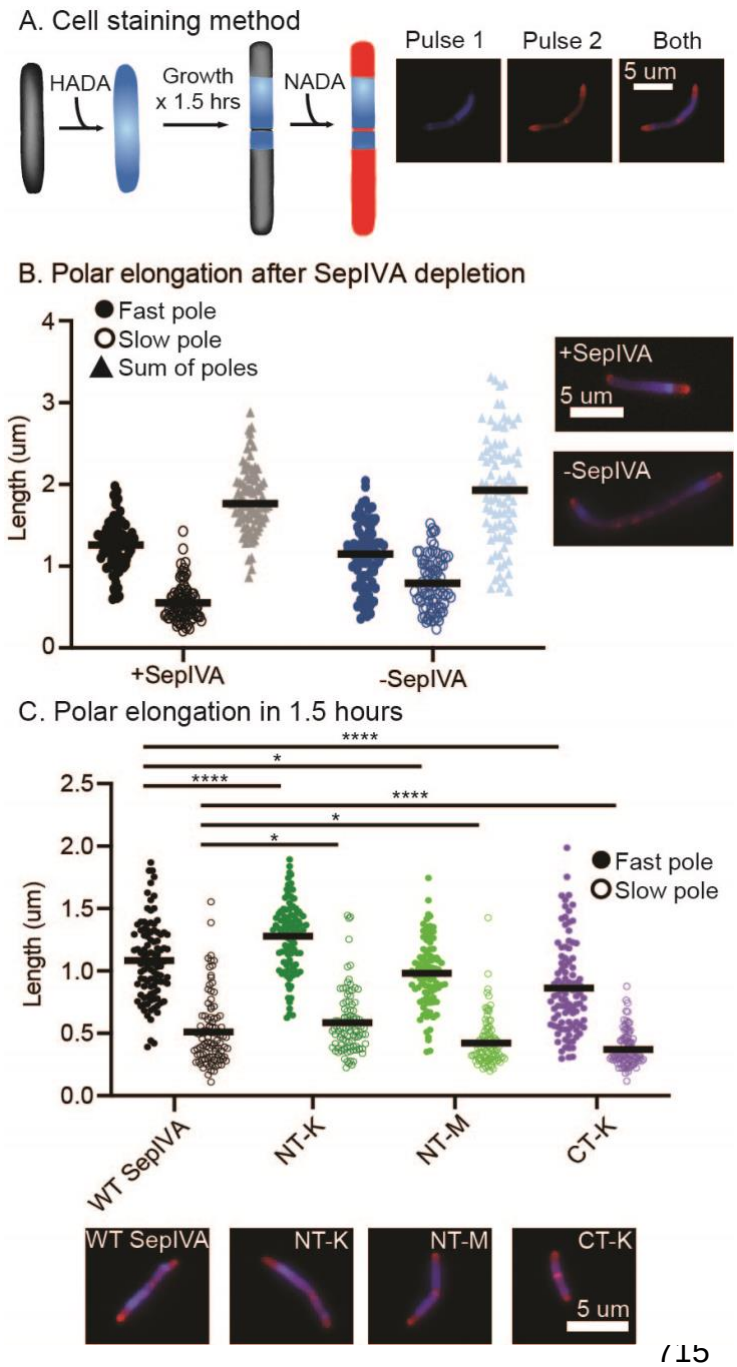

Figure 4. Arginine methylation of SepIVA affects polar elongation. (A) Schematic of pulse-chase-pulse staining method. **(B)** Length of poles after SepIVA depletion. Filled in dots represent the faster (brighter) growing pole, empty dots represent the slower (dimmer) growing pole. Triangles represent the sum of poles or total elongation. At least 100 cells across three biological replicates were analyzed. Bar represents median. Scale bar applies to all images. **(C)** Length of poles elongation after 1.5 hours in cells expressing L5::*sepIVA* WT and arginine methylation mutants. At least 100 cells across three biological replicates were analyzed. Bar represents median polar elongation. The adjusted p-values of each fast pole mutant compared to the WT are: NT-K = <0.0001; NT-M = 0.0458; and CT-K = <0.0001. The adjusted p-values of each slow pole mutant compared to the WT are: NT-K = 0.0446; NT-M = 0.0118; and CT-K = <0.0001. Representative cells are shown. Scale bar applies to all images. P-values

were calculated using ordinary one-way ANOVA, Dunnett's multiple comparisons test, with a single pooled variance in GraphPad Prism (v9.2).

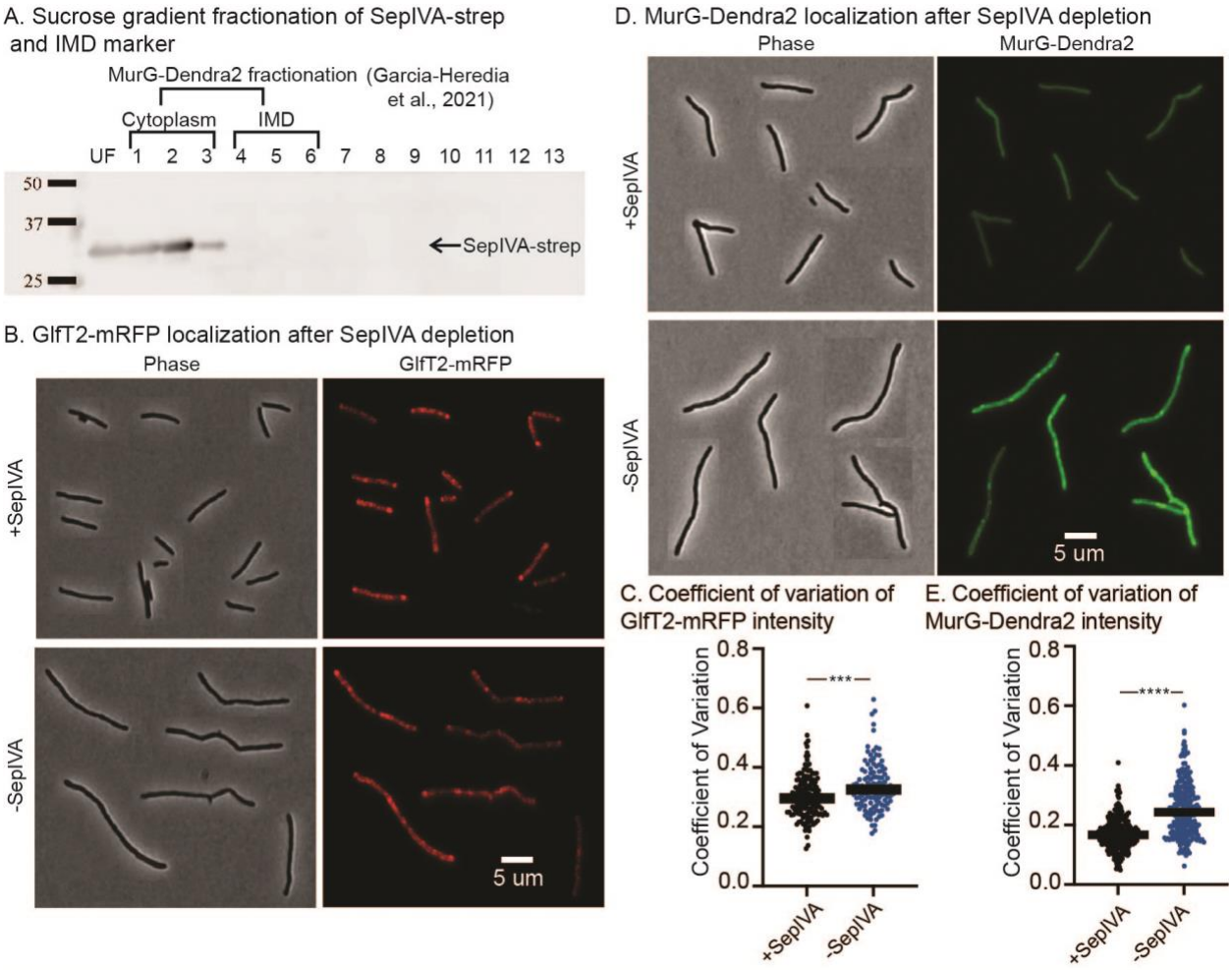

Figure 5. SepIVA has the same membrane association as MurG, and it affects MurG localization. (A) anti-Strep (top) western blot after sucrose gradient fractionations. Fractions 4-6 contain intracellular membrane domain (IMD) proteins. **(B)** Micrographs of cells expressing or depleting SepIVA and induced for GlfT2-mRFP. Scale bar is 5 microns and applies to all images. **(C)** GlfT2-mRFP distribution represented by coefficient of variation values. Coefficient of variation was calculated based on fluorescence intensity across the relative position of each cell. Bar represents median coefficient. **(D)** Micrographs of cells expressing or depleting SepIVA and induced for MurG-Dendra2. Scale bar is 5 microns and applies to all images. **(E)** MurG-

Dendra2 distribution represented by coefficient of variation values. Coefficient of variation was calculated based on fluorescence intensity across the relative position of each cell. Bar represents median coefficient. P-value calculated by unpaired t-test using GraphPad Prism (v9.2). Images of several cells were cropped together.

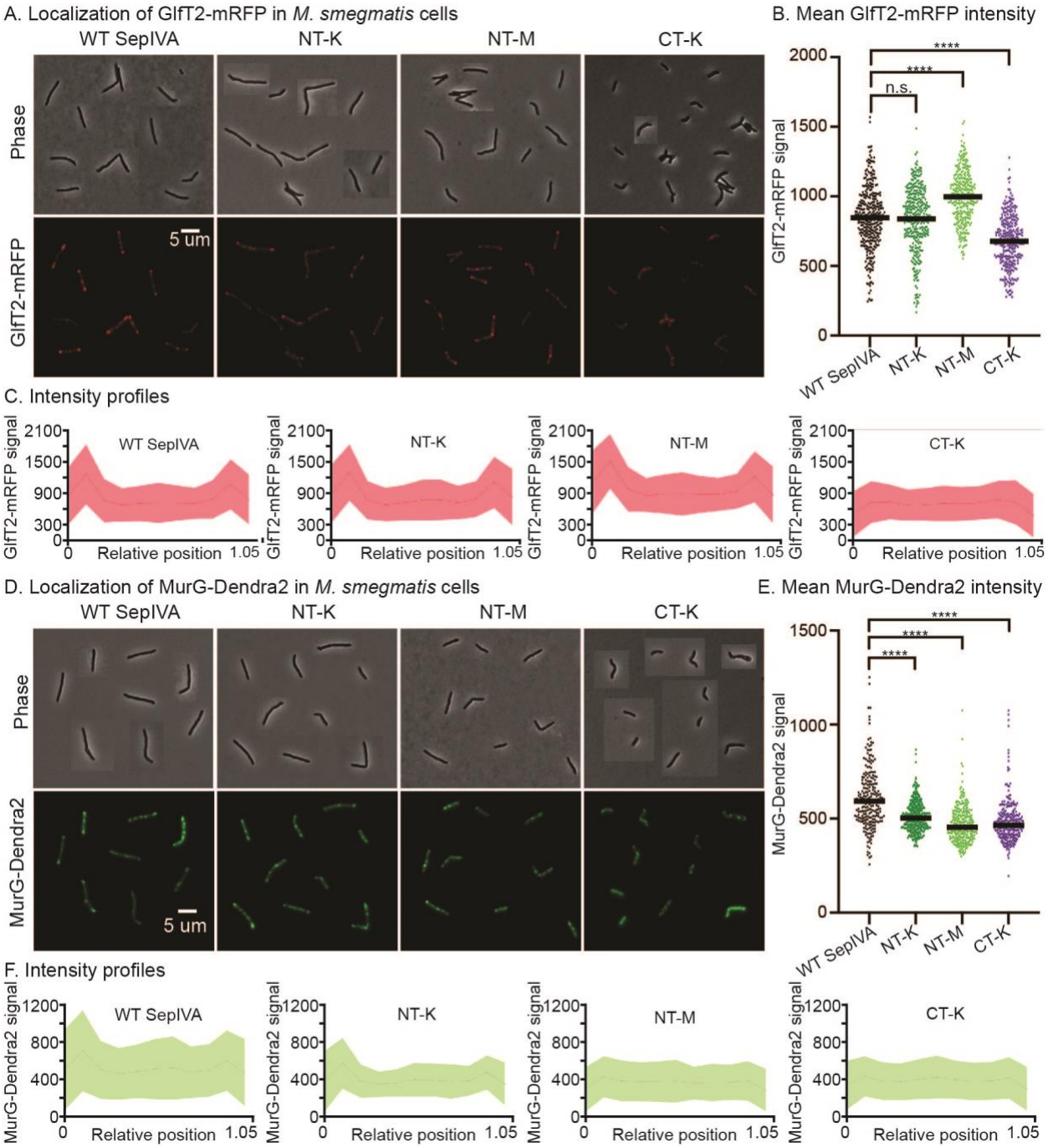
A. Localization of GlfT2-mRFP in M. smegmatis cells
WT SepIVA
NT-K
NT-M
CT-K
Phase
GlfT2-mRFP
5 um
B. Mean GlfT2-mRFP intensity
GlfT2-mRFP signal
n.s.
****
C. Intensity profiles
Relative position
D. Localization of MurG-Dendra2 in M. smegmatis cells
MurG-Dendra2
E. Mean MurG-Dendra2 intensity
MurG-Dendra2 signal
F. Intensity profiles

742

743

744

Figure 6. Arginine methylation of SepIVA affects MurG's localization to the poles. **(A)** Images of *M. smeg* cells expressing L5::*sepIVA* WT and arginine methylation mutants and induced for GlfT2-mRFP. Pictures of several cells from images processed identically were pasted together. Scale bar applies to all images. **(B)** Mean intensity values of 250+ cells expressing L5::*sepIVA* WT and arginine methylation mutants and induced for GlfT2-mRFP. Bar represents mean intensity value between cells. The adjusted p-values of each mutant compared to the WT are: NT-K = 0.9289; NT-M = <0.0001; and CT-K = <0.0001. At least 2 biological replicate strains were imaged for each genotype. **(C)** Intensity profiles of GlfT2-mRFP signal of WT and methylation mutants. The solid line represents the mean intensity value, and the shaded area represents standard deviation. At least 250+ cells across three biological replicates of each mutant were analyzed in MicrobeJ. Cells were pole-sorted such that the brighter pole in the HADA channel was set to 0 on the X axis. **(D)** Images of *M. smeg* cells expressing L5::*sepIVA* WT and arginine methylation mutants and TW::*murG-dendra2*. Pictures of several cells from images processed identically were pasted together. Scale bar applies to all images. **(E)** Mean intensity values of 250+ cells expressing L5::*sepIVA* WT and arginine methylation mutants and TW::*murG-dendra2*. Bar represents mean intensity value between cells. The adjusted p-values of each mutant compared to the WT are: NT-K = <0.0001; NT-M = <0.0001; and CT-K = <0.0001. Three biological replicate strains were imaged for each genotype. P-values were calculated using ordinary one-way ANOVA, Dunnett's multiple comparisons test, with a single pooled variance in GraphPad Prism (v9.2). **(F)** Intensity profiles of MurG-Dendra2 signal of WT and methylation mutants. The solid line represents the mean intensity value, and the shaded area represents standard deviation. At least 250+ cells across three biological replicates of each mutant were analyzed in MicrobeJ. Cells were pole-sorted such that the brighter pole in the HADA channel was set to 0 on the X axis. Images of several cells were cropped together.